Research Article | Vol. 26, No. 20 | 1 Oct 2018 | OPTICS EXPRESS 26750
Optics EXPRESS

# High-power OPCPA generating 1.7 cycle pulses at 2.5 µm

**N. BIGLER,* J. PUPEIKIS, S. HRISAFOV, L. GALLMANN, C. R. PHILLIPS, AND U. KELLER**

*Department of Physics, Institute for Quantum Electronics, ETH Zurich, August-Piccard-Hof 1 8093 Zurich, Switzerland*
**biglern@phys.ethz.ch*

**Abstract:** We present a high-power mid-infrared (mid-IR) optical parametric chirped-pulse amplifier (OPCPA) generating 14.4 fs pulses centered at 2.5 µm with an average power of 12.6 W and a repetition rate of 100 kHz. The short pulses are obtained without nonlinear pulse compression. This is in contrast to most few-cycle systems operating in the mid-IR. In our case, the ultrashort pulse duration is enabled by a careful design of the gain profile of each amplification stage as well as a precise control of the signal dispersion throughout the system. A pulse shaper is used in the seed beam to adjust the spectral phase at the output of the OPCPA system. This approach allows for a clean temporal profile leading to a high peak power of 6.3 GW.



## 1. Introduction

The laser source requirements for high-harmonic generation and attosecond science have been a key motivation for the development of high-power mid-infrared ultrafast laser sources [1,2]. Such experiments benefit from a high repetition rate, which raises the photon flux and therefore increases the signal-to-noise ratio or reduces the measurement time of experiments. Advances in high-repetition-rate ultrafast systems have enabled the extension of strong-field light-matter interactions into the hundreds of kilohertz to megahertz pulse-repetition-rate regime. Examples of corresponding applications are high-harmonic generation [3–5], the study of strong-field ionization with coincidence detection [6], or laser-based particle acceleration [7]. Another interest in the field is to move towards longer driving wavelength, which scales the high-harmonic cut-off and permits the generation of coherent soft-x-rays [8].

Optical parametric chirped-pulse amplification (OPCPA) [9,10] is an attractive approach to access the required parameters [11–18]. In this method, a narrow-band high-power pump pulse is used to amplify a broadband temporally chirped signal pulse. This allows for transferring the energy of standard multi-100-W class picosecond industrial lasers [19–21] to few-cycle pulses.

Achieving a high peak power at a high repetition rate in the mid-infrared (mid-IR) poses many technical challenges linked to thermal management, material limitations or nonlinear effects. Nonlinear self-compression is a promising method to obtain the ultrabroad bandwidth required for few-cycle pulses in the mid-IR spectral region [22–24]. This approach supports a bandwidth beyond an optical octave with a reduced acceptance bandwidth of the OPA crystals which gives more flexibility in the choice of nonlinear material and the intensity for high-power pumping. However, the resulting temporal pulse shape of such systems typically shows a large pedestal which reduces the achievable peak power.

Here we present a high-power mid-IR OPCPA system obtaining near-single-cycle bandwidth without nonlinear self-compression. We finely tune the gain bandwidth of every amplification stage to keep an ultrabroad bandwidth (from 1.7 to 3.2 µm) throughout the entire amplification chain. We obtain a pulse energy of 126 µJ at a pulse repetition rate of 100 kHz (12.6 W average power). The pulses are centered at a wavelength of 2.5 µm and have a

#341742 https://doi.org/10.1364/OE.26.026750
Journal © 2018 Received 7 Aug 2018; revised 18 Sep 2018; accepted 18 Sep 2018; published 28 Sep 2018

Optics EXPRESS

pulse duration of 14.4 fs (1.7 cycle), which is a record pulse duration for mid-IR systems with an average power above 10 W. Moreover, a pulse shaper based on a spatial light modulator allows for fine-tuning of the phase of the near-infrared seed pulse before the amplification chain. This leads to a clean compressed pulse, where the energy contained in the main peak can be maximized.

## 2. Setup

The complete system is pictured in Fig. 1 and is an upgrade of the system presented in [25]. We start with a carrier envelope offset (CEO) stabilized Ti:sapphire oscillator (Laser Quantum GmbH) generating pulses which are sufficiently broadband to seed the pump amplification chain as well as the OPCPA chain. A portion of the corresponding spectrum around 1030 nm is pre-amplified and pulsed-picked to 100 kHz using a set of acousto-optic modulators (AOMs), before being directed towards an Innoslab-type amplifier (Amphos GmbH). This produces 280 W average power with a full-width at half maximum (FWHM) pulse duration of 1.8 ps.

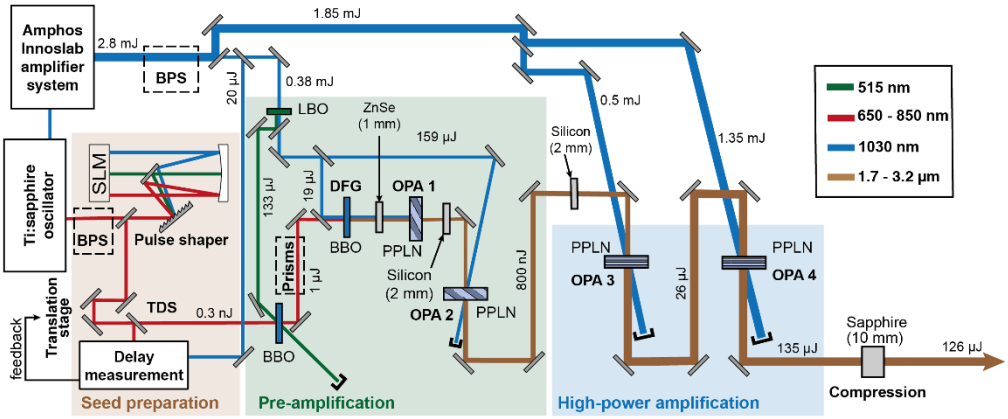


Fig. 1. The experimental setup. SLM: Spatial light modulator. BPS: Beam pointing stabilization. TDS: Time-delay stabilization. Prisms: SF10 prism pair stretcher. PPLN: Periodically poled $LiNbO_3$.

Part of the remaining near-infrared bandwidth from 640 to 930 nm is then selected and sent towards a 4-f pulse shaper based on a high-resolution liquid-crystal-on-silicon spatial light modulator (SLM, Meadowlark Optics Inc.) for fine-tuning of the spectral phase. We implemented a cross-correlation method to measure and correct for the delay drift between the signal and the pump [26]. Moreover, the beam pointing of both the signal and the pump were stabilized (TEM Messtechnik GmbH).

We split off 38 W of pump power for the pre-amplification part of the system. This beam is converted with 35% power efficiency to its second harmonic in a 1.5-mm-long LBO crystal. The 13.3 W of second-harmonic radiation is used to pre-amplify the signal in a 1.8-mm-long BBO crystal using a non-collinear geometry. We obtain 170 mW with a bandwidth spanning from 650 to 800 nm.

The rest of the pre-amplification chain is then pumped by the remaining fundamental from the second harmonic generation (SHG) stage. First, we overlap the near-infrared signal with 1.9 W of 1030-nm pump light in a difference-frequency generation (DFG) stage based on a 300-µm-long BBO crystal. As the pump and the signal both derive from the same CEO-stabilized oscillator, this could lead to inherently carrier-envelope-phase stable mid-IR pulse [27]. However, the AOMs used for pulse picking before amplification impose a frequency shift onto the seed of the Innoslab amplifier. The pump frequency comb being shifted by the AOMs driver frequency leads in turn to a mid-IR frequency comb with a non-zero CEO

Optics EXPRESS

frequency. This pump CEO frequency shift could be removed by phase-locking the driver frequency of the AOMs to the repetition-rate of the Ti:sapphire oscillator [28].

Since our system operates around strong water vapor absorption bands (1.8-1.95 and 2.5-2.9 µm), it is purged with nitrogen from the DFG stage onwards to reduce the effect of humidity in ambient air. The generated mid-IR idler is then directly amplified in a periodically poled MgO:LiNbO3 (MgO:PPLN, OPA 1). A large transversal component is added to the k-vector of the quasi-phase-matching (QPM) grating to impose additional momentum onto the degenerate mid-IR idler [25]. The remaining 15.9 W of pump power are then used in a second amplifier that is also relying on a noncollinear QPM grating to obtain 100 mW (1 µJ, 100 kHz) of near-infrared power. The design of the first and second pre-amplifier crystals are described in detail in [25].

The amplified mid-IR beam then enters the high-power amplification part of the system. For OPA 3 and 4 we use MgO:PPLN crystals with a wide QPM grating aperture of 10.9x2 $mm^2$ and a total crystal width of 14 mm (HC Photonics Corp.). The crystal thickness of 2 mm was chosen to be large enough to let the pump beam through at the targeted intensity, but otherwise minimized to improve the overall poling quality. Moreover, this wide aspect ratio allows for a predominantly one-dimensional heat flow, which permits a higher heat extraction. While little heat should be deposited unto the crystal during the OPA process, we still observe a temperature increase of the crystals during the first hour of operation. For example, in OPA 3 the temperature of the crystal holder typically rises by ~25 °C. This temperature change could derive from a combination of effects, such as two-photon absorption of the second harmonic of the pump or green-induced infrared absorption. While pump SHG is not nominally phase matched, it is still generated through a combination of near-phase-matching at high QPM orders and random duty cycle errors [29]. For better cooling performance, the crystals are mounted in a copper mount and sandwiched between two layers of 0.05-mm-thick indium foil. This increases both thermal and electrical contact, which should also lead to reduced photorefractive effects [30]. The QPM period used is 29.3 µm and the crystals are anti-reflection coated to achieve a low reflectivity at 515 nm, 1030 nm and between 1700 and 4700 nm. The crystals are operated at room temperature and pumped at a non-collinear angle of 3.5°.

The PPLN crystal of OPA 3 has a length of 1 mm and is pumped with 50 W of 1030-nm light. The pump beam is shaped to $1/e^2$ diameters of 1.50 mm vertically and 1.05 mm horizontally in order to reach a peak intensity of 33 $GW/cm^2$. This configuration leads to a gain of 18 dB and an output power of 3 W (30 µJ). The second power amplifier relies on a 0.5-mm-long PPLN crystal and is pumped with the remaining 135 W of pump power. The pump is shaped to $1/e^2$ diameters of 4.85 mm vertically and 1.2 mm horizontally leading to a peak intensity of 24 $GW/cm^2$. We amplify the mid-IR signal to 13.5 W (gain of 7 dB, pulse energy of 135 µJ at 100 kHz).

## 3. Dispersion and bandwidth management

As pointed out above, the design goal of this system was to generate a high-power ultra-broadband mid-IR bandwidth without relying on nonlinear spectral broadening, in order to obtain few-cycle pulses which can be compressed and shaped via the pulse shaper at the input side of the system. To do so, it is not only necessary to start with a broadband seed, but this bandwidth must also be maintained throughout the entire amplification chain. In OPCPA, shaping of the spectral gain is generally governed by two effects: phase matching and temporal coupling.

The spectral narrowing effect due to imperfect phase matching can usually be mitigated by using sufficiently short crystals, which extends the amplified bandwidth at the cost of necessitating a higher pump intensity. Another common method to increase the gain bandwidth is to operate away from perfect phase-matching by shifting the wavevector mismatch curve through the $\Delta k = 0$ point [Fig. 2(a)] [13]. If this curve displays a turning

Optics EXPRESS

point, a broad spectral gain profile with two peaks at the edges of the bandwidth and a reduced gain in the center is obtained, as shown in Fig. 2(b).

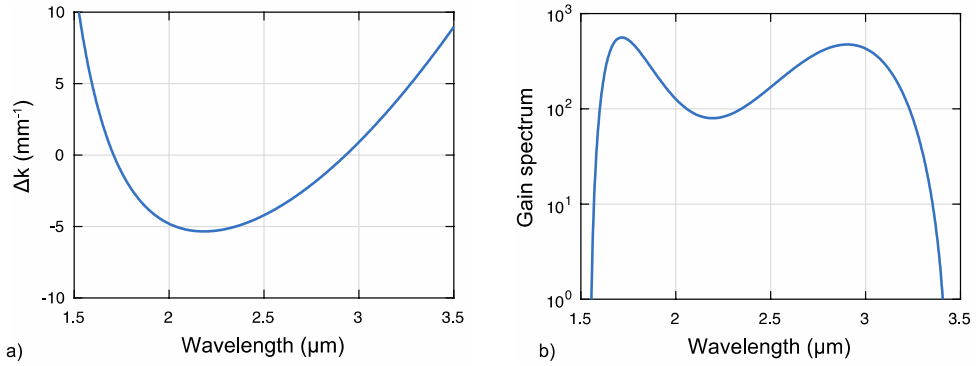


Fig. 2. (a) Example of a detuned wavevector mismatch curve. The non-collinear angle between the signal and the pump is 3°, the QPM period is 29.5 μm and the pump wavelength is 1030 nm. The Sellmeier relation used in this calculation is taken from Gayer et al. [31] (b) Calculated gain spectrum for the wavevector mismatch shown in (a). The pump intensity is 15 GW/cm$^2$ and the crystal length is 1 mm. If the wavevector mismatch curve displays a turning point, two maxima appear in the gain spectrum for wavelengths where $\Delta k = 0$, leading to a larger gain in the wings than in the center of the bandwidth.

On the other hand, the pump temporal profile will behave as a spectral filter as soon as the signal is sufficiently chirped. The part of the signal spectrum overlapped with the peak of the pump (for linearly chirped pulses, this will be the center of the bandwidth) will see a larger gain than the parts overlapped with the beginning or the end of the pump pulse. This effect is particularly important in the high-gain regime, when pump saturation does not play a prominent role.

Most materials show a positive third-order dispersion (TOD) in the mid-IR spectral range, whereas second-order dispersion can have an opposite sign for different materials (for example silicon and sapphire). Therefore, to support linear compression in bulk material, the output of OPA 4 needs to have a significant negative TOD. In Fig. 3(a), we show the group delay curves for the signal beam before each amplifier. The system is designed such that a spectrally flat group delay is obtained after propagation through 10 mm of sapphire at the output of the system. The thus required negative TOD is apparent for each stage. In order to introduce this negative TOD, we implemented a prism compressor in the near-infrared beam path just before the DFG stage using SF10 prisms separated by 37.5 cm. This leads to a chirp dominated by TOD in the DFG and OPA 1. The pulses are then chirped between the different amplification stages using a combination of zinc selenide and silicon windows oriented at Brewster angle to reduce reflection losses (see Fig. 1). We make sure that TOD dominated chirp turns into a mainly linear chirp (no turning point in the group delay curve within the signal bandwidth) before reaching the high-power part of the system to ensure a limited cross-talk between the different parts of the amplified spectrum.

To maintain the entire signal bandwidth throughout the system, we first detune the phase-matching in the first two mid-IR OPAs (where the signal is not linearly chirped) in order to achieve a larger gain in the spectral wings of the signal bandwidth compared to its center, as displayed in Fig. 3(b). The signal is then chirped before OPA 3 [see Fig. 3(a)]. The monotonic group delay vs frequency curve means that the center of the signal spectrum is overlapped with the center of the pump temporal profile. This in turn leads to a larger gain in the center of the spectrum than in the wings for the two remaining OPAs, allowing to recover the middle part of the spectrum.

Finally, the signal chirp is compensated by the material dispersion of an anti-reflection coated 10-mm-long sapphire crystal. After compression, we obtain an average output power

Optics EXPRESS

of 12.6 W (126 µJ pulse energy, 100 kHz repetition rate). Any remaining spectral phase distortion is removed using the pulse shaper in the near-infrared section of the system.

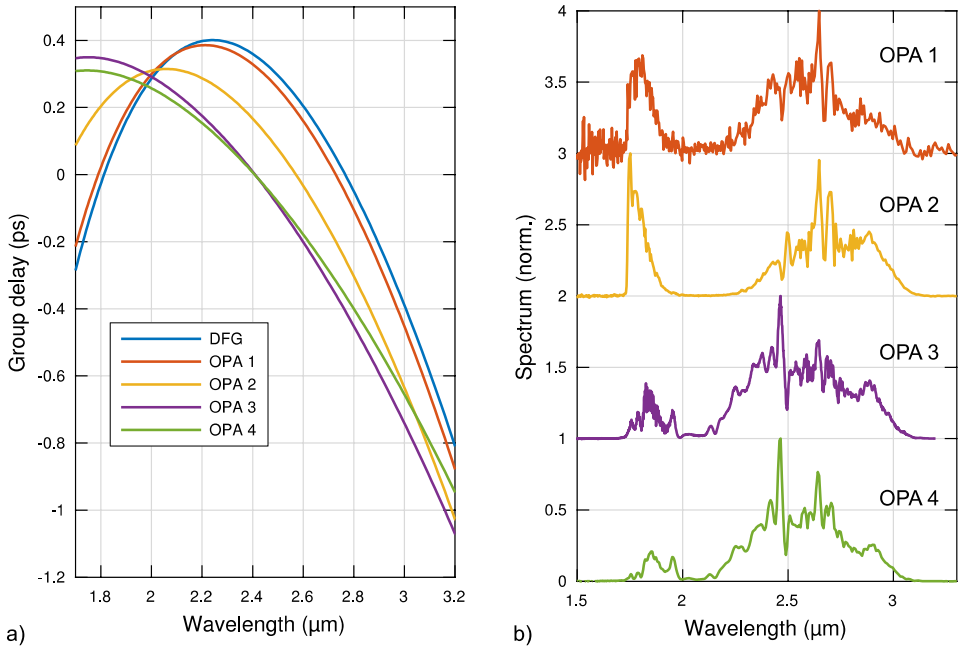


Fig. 3. (a) The predicted group delay curves before the different nonlinear stages. A large negative TOD is first applied to the pulses before the DFG stage, to allow for a final compression in bulk sapphire. The pulses are then chirped sufficiently to remove any turning point in the group delay curve within the amplified spectrum before the high-power amplification part of the system. (b) The spectra measured after each mid-IR OPA stages. All spectra were measured with a scanning MIR spectrometer based on an acousto-optic modulator (MOZZA, Fastlite).

## 4. High-power result

Because of the high pump power and intensity used, unwanted nonlinear processes strongly affect the transmitted pump beam profile in both OPA 3 and OPA 4. Because of this, we chose to use separate pump beams for these two stages (50 W and 135 W, respectively), rather than sending the full 185 W beam through OPA 3 and then reusing the transmitted power for OPA 4 (which would be favorable for power extraction). To demonstrate these effects, Fig. 4(a) shows the transmitted pump beam through OPA 4 at low power (30 W, 5 GW/cm$^2$), with the input signal being blocked. In Fig. 4(b), the pump power is increased to 110 W (19 GW/cm$^2$). Two effects can be observed.

First, the beam shows the appearance of a fine structure in the direction perpendicular to the crystal c-axis. This is not the result of the Kerr effect as the B-integral remains below 0.25 rad. However, further investigation is needed to determine the specific mechanism leading to this structure. The second pump beam distorting effect is a spatial broadening of the beam along the direction of the crystal c-axis, which is typical of the photorefractive effect [32].

Both of these processes clamp the available gain, likely due to a combination of reduced spatial overlap between the signal and the pump and a phase-mismatch contribution associated with the photorefractive effects. At high power, the amplified signal shows signs of broadening along the crystal c-axis but no sign of the fine beam structure [see Fig. 4(c)]. The remaining distortion was corrected by using separate cylindrical telescopes for the horizontal and the vertical axis.

Optics EXPRESS

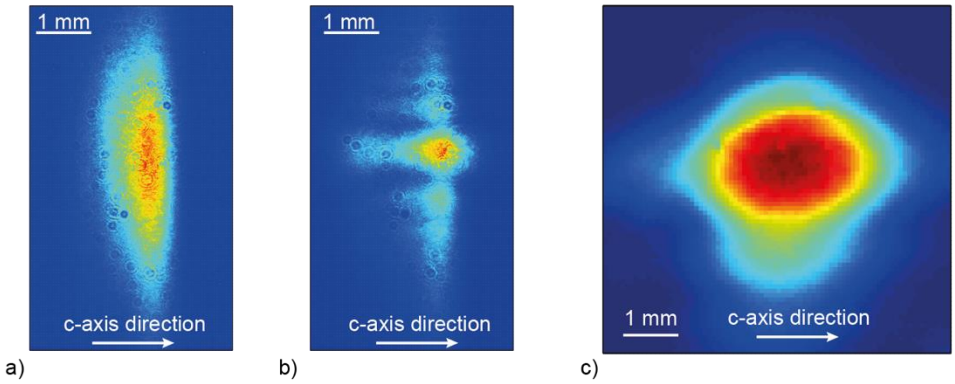


Fig. 4. (a) The pump profile after transmission through OPA 4 with 30 W of average power. The pump is measured 50 cm after the PPLN crystal. (b) The pump profile after transmission through OPA 4 with 110 W of average power. Two concurrent effects can be observed: a spatial broadening along the crystal c-axis and the appearance of a rapid modulation along the other axis (see text). (c) The amplified signal profile, measured with a pyroelectric camera (Pyrocam III, Ophir Optronics Solutions Ltd.). The signal is first reshaped with two cylindrical telescopes before being directed towards the camera.

After OPA 4 we obtain an average output power of 13.5 W (135 µJ, 100 kHz, measured before the chirp compensation), with a standard deviation of 0.06 W or 0.5% measured over 5 minutes, as shown on Fig. 5(a). We do not observe any sign of optical parametric generation when blocking the signal at the beginning of the amplification chain. Furthermore, the amplified signal shows no sign of spatial or angular chirp. We also investigated potential coupling between different spectral components of the signal by blocking part of the spectrum at the pulse shaper position. We did not observe any form of cross-talk between the long- and short-wavelength side of the spectrum.

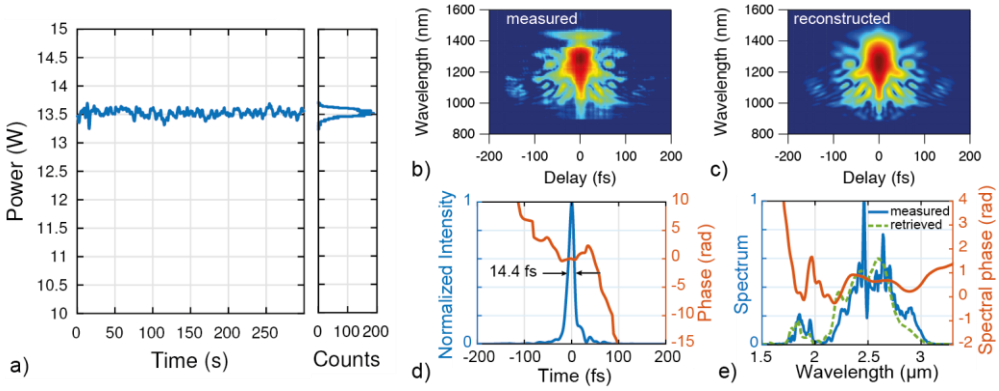


Fig. 5. (a) The output power measured after OPA 4 and before the chirp compensation in bulk sapphire, measured over 5 minutes. (b) The measured SHG-FROG trace. (c) The reconstructed SHG-FROG trace. The reconstruction uses a grid of 512x512 points with a temporal resolution of 1.28 fs and a frequency resolution of 1.52 THz. We obtain a root mean square reconstruction error of 0.5%. (d) The retrieved temporal profile. We measure a full-width at half-maximum pulse duration of 14.4 fs, close to the transform limit of 13.2 fs. (e) The retrieved spectrum and spectral phase, along with an independently measured fundamental spectrum.

## 5. Temporal characterization

The pulse duration is measured in a home built SHG-FROG setup based on a 20-µm-long BBO crystal (Newlight Photonics Inc.). The measured trace is displayed in Fig. 5(b) while the

Optics EXPRESS

reconstructed trace is shown in Fig. 5(c). The measured trace was post-processed following Baltuskas et al. [33]. The BBO crystal used is sufficiently thin so that the phase-matching term in the correction factor is sufficiently small to be neglected. Figure 5(d) shows the extracted temporal profile and Fig. 5(e) the retrieved spectrum and spectral phase along with an independently measured spectrum. We obtain a full-width at half-maximum pulse duration of 14.4 fs at a central wavelength of 2.5 µm, which corresponds to 1.7 cycles.

The pulse shaper allows for very precise tuning of the remaining phase, leading to a pulse duration very close to the transform limit of 13.2 fs. Moreover, another advantage of this method compared to pulse shortening through nonlinear compression is that it allows maximizing the energy contained within the main peak of the pulse. This leads to a high peak power of 6.3 GW, close to the 8.2 GW of a Gaussian pulse with the same duration and energy.

## 6. Conclusion

We presented a high-power mid-IR ultrafast OPCPA system generating 126-µJ pulses centered at 2.5 µm with a duration of 14.4 fs (1.7 cycles). This pulse duration is achieved without nonlinear pulse compression, leading to a clean temporal profile and therefore a high peak power. Moreover, the group delay is carefully managed over the entire signal bandwidth so that the pulses can be directly recompressed in bulk sapphire, resulting in the high transmission efficiency of 93%. The high-power part of the system relies on MgO:PPLN, demonstrating that such crystals are well suited for amplification with a pump power exceeding 100 W. Further development of this system will include the implementation of CEP stabilization.

This unique ultrafast high-power mid-IR source will serve as the pump for a high-flux high-harmonic-generation beamline generating photons in the water window. It represents a key enabling step for mid-IR driven attosecond science.

## Funding

H2020 European Research Council (ERC Advanced Grant AttoClock-320401); Swiss National Science Foundation (SNSF) projects (200021_159975 and 200020_172644).

## References

1. U. Keller, “Recent developments in compact ultrafast lasers,” Nature **424**(6950), 831–838 (2003).
2. T. Südmeyer, S. V. Marchese, S. Hashimoto, C. R. E. Baer, G. Gingras, B. Witzel, and U. Keller, “Femtosecond laser oscillators for high-field science,” Nat. Photonics **2**(10), 599–604 (2008).
3. S. Hädrich, J. Rothhardt, M. Krebs, S. Demmler, A. Klenke, A. Tünnermann, and J. Limpert, “Single-pass high-harmonic generation at high repetition rate and photon flux,” J. Phys. B **49**, 17 (2016).
4. F. Emaury, A. Diebold, C. J. Saraceno, and U. Keller, “Compact extreme ultraviolet source at megahertz pulse repetition rate with a low-noise ultrafast thin-disk laser oscillator,” Optica **2**(11), 980–984 (2015).
5. E. Lorek, E. W. Larsen, C. M. Heyl, S. Carlström, D. Paleček, D. Zigmantas, and J. Mauritsson, “High-order harmonic generation using a high-repetition-rate turnkey laser,” Rev. Sci. Instrum. **85**(12), 123106 (2014).
6. J. Rothhardt, S. Hädrich, Y. Shamir, M. Tschnernajew, R. Klas, A. Hoffmann, G. K. Tadesse, A. Klenke, T. Gottschall, T. Eidam, J. Limpert, A. Tünnermann, R. Boll, C. Bomme, H. Dachraoui, B. Erk, M. Di Fraia, D. A. Horke, T. Kierspel, T. Mullins, A. Przystawik, E. Savelyev, J. Wiese, T. Laarmann, J. Küpper, and D. Rolles, “High-repetition-rate and high-photon-flux 70 eV high-harmonic source for coincidence ion imaging of gas-phase molecules,” Opt. Express **24**(16), 18133–18147 (2016).
7. E. A. Peralta, K. Soong, R. J. England, E. R. Colby, Z. Wu, B. Montazeri, C. McGuinness, J. McNeur, K. J. Leedle, D. Walz, E. B. Sozer, B. Cowan, B. Schwartz, G. Travish, and R. L. Byer, “Demonstration of electron acceleration in a laser-driven dielectric microstructure,” Nature **503**(7474), 91–94 (2013).
8. T. Popmintchev, M.-C. Chen, D. Popmintchev, P. Arpin, S. Brown, S. Ališauskas, G. Andriukaitis, T. Balčiunas, O. D. Mücke, A. Pugzlys, A. Baltuška, B. Shim, S. E. Schrauth, A. Gaeta, C. Hernández-García, L. Plaja, A. Becker, A. Jaron-Becker, M. M. Murnane, and H. C. Kapteyn, “Bright coherent ultrahigh harmonics in the keV x-ray regime from mid-infrared femtosecond lasers,” Science **336**(6086), 1287–1291 (2012).
9. A. Dubietis, G. Jonusauskas, and A. Piskarskas, “Powerful femtosecond pulse generation by chirped and strechted pulse parametric amplification in BBO crystal,” Opt. Commun. **88**(4-6), 437–440 (1992).
10. S. Witte and K. S. E. Eikema, “Ultrafast optical parametric chirped-pulse amplification,” IEEE J. Sel. Top. Quantum Electron. **18**(1), 296–307 (2012).

Optics EXPRESS


11. M. Neuhaus, H. Fuest, M. Seeger, J. Schötz, M. Trubetskov, P. Russbueldt, H. D. Hoffmann, E. Riedle, Z. Major, V. Pervak, M. F. Kling, and P. Wnuk, "10 W CEP-stable few-cycle source at 2 μm with 100 kHz repetition rate," Opt. Express **26**(13), 16074–16085 (2018).
12. B. W. Mayer, C. R. Phillips, L. Gallmann, and U. Keller, "Mid-infrared pulse generation via achromatic quasi-phase-matched OPCPA," Opt. Express **22**(17), 20798–20808 (2014).
13. Y. Deng, A. Schwarz, H. Fattahi, M. Ueffing, X. Gu, M. Ossiander, T. Metzger, V. Pervak, H. Ishizuki, T. Taira, T. Kobayashi, G. Marcus, F. Krausz, R. Kienberger, and N. Karpowicz, "Carrier-envelope-phase-stable, 1.2 mJ, 1.5 cycle laser pulses at 2.1 μm," Opt. Lett. **37**(23), 4973–4975 (2012).
14. A. Thai, M. Hemmer, P. K. Bates, O. Chalus, and J. Biegert, "Sub-250-mrad, passively carrier-envelope-phase-stable mid-infrared OPCPA source at high repetition rate," Opt. Lett. **36**(19), 3918–3920 (2011).
15. N. Thiré, R. Maksimenka, B. Kiss, C. Ferchaud, P. Bizouard, E. Cormier, K. Osvay, and N. Forget, "4-W, 100-kHz, few-cycle mid-infrared source with sub-100-mrad carrier-envelope phase noise," Opt. Express **25**(2), 1505–1514 (2017).
16. B. W. Mayer, C. R. Phillips, L. Gallmann, M. M. Fejer, and U. Keller, "Sub-four-cycle laser pulses directly from a high-repetition-rate optical parametric chirped-pulse amplifier at 3.4 μm," Opt. Lett. **38**(21), 4265–4268 (2013).
17. P. Rigaud, A. Van de Walle, M. Hanna, N. Forget, F. Guichard, Y. Zaouter, K. Guesmi, F. Druon, and P. Georges, "Supercontinuum-seeded few-cycle mid-infrared OPCPA system," Opt. Express **24**(23), 26494–26502 (2016).
18. B. M. Luther, K. M. Tracy, M. Gerrity, S. Brown, and A. T. Krummel, "2D IR spectroscopy at 100 kHz utilizing a Mid-IR OPCPA laser source," Opt. Express **24**(4), 4117–4127 (2016).
19. P. Russbueldt, T. Mans, J. Weitenberg, H. D. Hoffmann, and R. Poprawe, "Compact diode-pumped 1.1 kW Yb:YAG Innoslab femtosecond amplifier," Opt. Lett. **35**(24), 4169–4171 (2010).
20. J.-P. Negel, A. Loescher, A. Voss, D. Bauer, D. Sutter, A. Killi, M. A. Ahmed, and T. Graf, "Ultrafast thin-disk multipass laser amplifier delivering 1.4 kW (4.7 mJ, 1030 nm) average power converted to 820 W at 515 nm and 234 W at 343 nm," Opt. Express **23**(16), 21064–21077 (2015).
21. C. J. Saraceno, F. Emaury, C. Schriber, M. Hoffmann, M. Golling, T. Südmeyer, and U. Keller, "Ultrafast thin-disk laser with 80 μJ pulse energy and 242 W of average power," Opt. Lett. **39**(1), 9–12 (2014).
22. U. Elu, M. Baudisch, H. Pires, F. Tani, M. H. Frosz, F. Köttig, A. Ermolov, P. St. J. Russell, and J. Biegert, "High average power and single-cycle pulses from a mid-IR optical parametric chirped pulse amplifier," Optica **4**, 1024–1029 (2017).
23. A. A. Lanin, A. A. Voronin, E. A. Stepanov, A. B. Fedotov, and A. M. Zheltikov, "Multioctave, 3-18 μm sub-two-cycle supercontinua from self-compressing, self-focusing soliton transients in a solid," Opt. Lett. **40**(6), 974–977 (2015).
24. V. Shumakova, P. Malevich, S. Ališauskas, A. Voronin, A. M. Zheltikov, D. Faccio, D. Kartashov, A. Baltuška, and A. Pugžlys, "Multi-millijoule few-cycle mid-infrared pulses through nonlinear self-compression in bulk," Nat. Commun. **7**, 12877 (2016).
25. N. Bigler, J. Pupeikis, S. Hrisafov, L. Gallmann, C. R. Phillips, and U. Keller, "Decoupling phase-matching bandwidth and interaction geometry using non-collinear quasi-phase-matching gratings," Opt. Express **26**(5), 6036–6045 (2018).
26. S. Prinz, M. Häfner, M. Schultze, C. Y. Teisset, R. Bessing, K. Michel, R. Kienberger, and T. Metzger, "Active pump-seed-pulse synchronization for OPCPA with sub-2-fs residual timing jitter," Opt. Express **22**(25), 31050–31056 (2014).
27. A. Baltuska, T. Fuji, and T. Kobayashi, "Controlling the carrier-envelope phase of ultrashort light pulses with optical parametric amplifiers," Phys. Rev. Lett. **88**(13), 133901 (2002).
28. O. de Vries, T. Saule, M. Plötner, F. Lücking, T. Eidam, A. Hoffmann, A. Klenke, S. Hädrich, J. Limpert, S. Holzberger, T. Schreiber, R. Eberhardt, I. Pupeza, and A. Tünnermann, "Acousto-optic pulse picking scheme with carrier-frequency-to-pulse-repetition-rate synchronization," Opt. Express **23**(15), 19586–19595 (2015).
29. C. R. Phillips, J. S. Pelc, and M. M. Fejer, "Parametric processes in quasi-phasematching gratings with random duty cycle errors," J. Opt. Soc. Am. B **30**(4), 982–993 (2013).
30. J. R. Schwesyg, M. Falk, C. R. Phillips, D. H. Jundt, K. Buse, and M. M. Fejer, "Pyroelectrically induced photorefractive damage in magnesium-doped lithium niobate crystals," J. Opt. Soc. Am. B **28**(8), 1973–1987 (2011).
31. O. Gayer, Z. Sacks, E. Galun, and A. Arie, "Temperature and wavelength dependent refractive index equations for MgO-doped congruent and stoichiometric LiNbO3," Appl. Phys. B **91**(2), 343–348 (2008).
32. A. Ashkin, G. D. Boyd, J. M. Dziedzic, R. G. Smith, A. A. Ballman, J. J. Levinstein, and K. Nassau, "Optically-induced refractive index inhomogeneities in LiNbO3 and LiTaO3," Appl. Phys. Lett. **9**(1), 72–74 (1966).
33. A. Baltuska, M. S. Pshenichnikov, and D. A. Wiersma, "Second-harmonic generation frequency-resolved optical gating in the single-cycle regime," IEEE J. Quantum Electron. **35**(4), 459–478 (1999).